Electron transport in a gold nanoparticle assembly structure stabilized by a physisorbed porphyrin derivative

Yuki Noda,[1] Shin-ichiro Noro,[1,2] Tomoyuki Akutagawa,[3] and Takayoshi Nakamura[1,2]
[1]*Graduate School of Environmental Science, Hokkaido University, N10W5, Kita-ku, Sapporo 060-0810, Japan*
[2]*Research Institute for Electronic Science, Hokkaido University, N20W10, Kita-ku, Sapporo 001-0020, Japan*
[3]*Institute of Multidisciplinary Research for Advanced Materials, Tohoku University, 1-1 Katahira, 2-Chome, Sendai 980-8577, Japan*
(Received 1 July 2010; revised manuscript received 1 October 2010; published 12 November 2010)

Gold nanoparticles stabilized by *meso*-5,10,15,20-tetrakis(2-thienyl)porphyrin (2T) via physisorption (2T-AuNP) were synthesized, and the electronic transport of assemblies of these films was studied. The adsorption mechanism of 2T on gold nanoparticles was examined using UV-vis-NIR, IR, Raman, and ^{1}H-NMR spectroscopy, which showed no evidence of any covalent bonding between 2T and the gold nanoparticles. In temperature-dependent resistivity measurements, a crossover from thermally assisted hopping to Efros-Shklovskii-type variable-range hopping (ES-VRH) was observed around 50 K on decreasing the temperature. At higher temperatures, the 2T-AuNP assembly structure followed an Arrhenius plot (E_A=15 meV) with ohmic *I-V* characteristics at each measurement point. On the other hand, the activation energy at lower temperatures decreased nonlinearly in a T^{-1} plot, and the logarithm of the resistance obeyed a $T^{-1/2}$ law, corresponding to an ES-VRH mechanism, which is predicted for disordered materials as a variable-range hopping mechanism influenced by strong Coulomb interactions. ES-VRH behavior has been observed previously in saturated molecule/gold nanoparticle assemblies and was confirmed in our 2T-AuNP assembly. Electronically active conjugated molecules were successfully incorporated between the nanoparticles, keeping the electronic structure of the gold nanoparticle and 2T moieties isolated from each other.

DOI: 10.1103/PhysRevB.82.205420 PACS number(s): 72.80.Tm

I. INTRODUCTION

Gold nanoparticle assemblies have attracted much attention because they are predicted to act as building blocks for new electronic devices. A number of studies have been carried out to connect gold nanoparticles with organic molecules, and the electron transport properties of the resulting network structures have been evaluated. For example, gold nanoparticle saturated alkane assemblies show metal-insulator transitions, depending on the strength of the internanoparticle coupling, which is regulated by the internanoparticle separation distance.[1] Normal and inverse photoconductivity has been observed by irradiation using visible light close to the surface-plasmon resonance of the gold nanoparticles.[2] Spin-polarized molecular wires connecting the gold nanoparticles showed negative magnetoresistance behavior.[3] The electron transport properties of the assembled gold nanoparticles are strongly dependent on the assembly structure, as well as on the organic molecules connecting the nanoparticles. A wide range of conduction models has been proposed so far.

Protecting ligands, such as sulfur, phosphine, citrate, amine, carboxylate, and isocyanide groups have been used to stabilize the gold nanoparticles. Among these, sulfur-stabilized gold nanoparticles have been widely applied, because they allow for the facile synthesis of thermally stable particles with a narrow size dispersion, and the incorporation of a conjugated molecule is possible by utilizing the strong covalent bonds between the Au and S atoms.[4] Investigations into the electron transport properties of gold nanoparticle assemblies have been mainly carried out on Au-S-stabilized nanoparticles. For example, Torma *et al.*[5] have reported on the influence of chemical bonds on the activation energy using covalent or noncovalently linked gold nanoparticle assemblies employing saturated alkyl dithiolate or thiolate ligands, respectively. For noncovalently linked nanoparticles, the activation energy shows a linear relationship with internanoparticle distance, with a minor dependence on the chemical structure of the linker molecules. On the other hand, covalently linked nanoparticles show a nonlinear relationship with the internanoparticle distance. The latter results suggest that the molecular orbitals of the linking molecules play an important role in the electron transport properties of the gold nanoparticle assemblies. Wessels *et al.*[6] have studied the conductivity of gold nanoparticle assemblies from the viewpoint of the conjugation strength of the molecules. They found that the conductivity exhibited an exponential decay versus the number of nonconjugated bonds in the linker molecule, suggesting that these molecules can be viewed as being serial connections of electrically insulating (nonconjugated) and conductive (conjugated) parts.

Selection of the binding groups connecting the molecules to the nanoparticle is also important for the electron transport. Chen *et al.*[7] reported on the effect of the binding group on the single-molecule conductivity on an Au(111) surface using an Au scanning tunnel microscope tip. They found that the contact resistance, representing the strength of the electronic coupling between the molecules and the electrode, was very sensitive to the binding group, which decreased in the order: thiol (-SH) > amine (-NH_2) > carboxylic acid (-COOH), although the tunneling decay constant representing the efficiency of the electron transport was not dependent on the binding group.

In general, if a strong electronic coupling between a molecule and an electrode is realized, as in the case of Au-S bonds having a large polarization field at the metal-molecule

interface, then the energy levels in the molecule broaden and the intrinsic electronic structure becomes ambiguous.[8] If a molecule is adsorbed on a metal's surface with weak physisorption rather than strong chemisorption, the tunneling of electrons between the nanoparticles should be dominated by the intrinsic electronic structure of the molecule.

An assembly of gold nanoparticles protected by an electronically active conjugated molecule coupled with noncovalent bonding is an ideal system to study the effect of molecular structure and the frontier orbitals on the single electron conduction between gold nanoparticles, because it avoids a contribution from the binding groups, and reflects the contribution of the intrinsic electronic structure of the molecules and gold nanoparticles on the electron transport properties.

In this work, we have synthesized gold nanoparticles protected by a porphyrin derivative coupled via physisorption. *meso*-5,10,15,20-tetrakis(2-thienyl)porphyrin (2T) was selected for this purpose, because of its electronically active conjugated system, as well as its planar and robust structure. Gold nanoparticles protected by 2T (2T-AuNP) were assembled and the temperature-dependent electron transport properties were investigated. The 2T-AuNP assembly films showed a crossover around 50 K occurred from an Arrhenius-type thermally assisted hopping mechanism to an Efros-Shklovskii-type variable-range hopping (ES-VRH) mechanism with a strong Coulomb interaction regime.

II. EXPERIMENTAL

A. Synthesis of 2T-AuNP

The *meso*-5,10,15,20-tetrakis(2-thienyl)porphyrin used was synthesized using a method described in the literature.[9] Preparation of the gold nanoparticles protected by 2T was carried out in a two-phase system, as described by Brust *et al.*[4] A volume of 70 ml of an aqueous solution of $HAuCl_4$ $3H_2O$ (252 mg, 0.64 mmol) was mixed with 210 ml of a toluene solution of tetraoctylammonium bromide (TOAB). The two phases were stirred until all the tetrachloroaurate had transferred into the toluene phase. Then, 105 ml of a toluene solution of 2T (98 mg, 0.15 mmol) was added, and the mixture was stirred for a period of 15 min. Finally, 10 ml of an aqueous solution of $NaBH_4$ (105 mg, 2.77 mmol) was added slowly. After stirring for a further 20 min, the toluene phase was separated and concentrated. Ethanol was then added, and the resulting precipitate was washed with ethanol and toluene to obtain gold nanoparticles protected by 2T (2T-AuNP).

Elemental analysis of the 2T-AuNP showed C:H:N:S =6.08%:0.72%:0.54%:1.05%, which corresponded to a ratio of 2T:gold atoms of 1:33. The cross-sectional area of 2T for the flat and edge-on configurations was estimated from the molecular model compiled by the MERCURY and IMAGEJ (Ref. 10) [Fig. S1 (Ref. 11)]. Geometry optimization of 2T was carried out using density-functional theory calculations employing the B3LYP model with a 6-31G(d) basis set performed using the GAUSSIAN 03 software package.[12]

B. Characterization of 2T-AuNP

The average diameter of the gold nanoparticles was examined using transmission electron microscopy (TEM) and small-angle x-ray scattering (SAXS) in solution [see Fig. S2 (Ref. 11)]. TEM measurements were carried out using a Hitachi HD-2000 TEM employing an acceleration voltage of 200 kV. Samples for the TEM measurements were prepared on a carbon-coated Cu grid (Okenshoji Co. Ltd., Japan) by drop casting a toluene solution of the 2T-AuNP suspension, and then allowing the toluene to evaporate. The results were in good agreement with the SAXS data. The SAXS data were measured using a Rigaku Nanoviewer IP diffractometer employing Cu $K\alpha$ radiation ($\lambda=1.5418$ Å) and a graphite monochromator (40 kV, 30 mA). A *N*,*N*-dimethylformamide (DMF) solution of the gold nanoparticles was measured in the transmittance SAXS mode and the scattering profile was analyzed using the Rigaku GXRR software package. An average diameter of the 2T-AuNPs of 4.0 nm and a normalized variance of 10.3% were obtained using the least-squares method over a scanning range of 0.5 to 4.0° using a structural factor of unity [Fig. S3 (Ref. 11)].

UV-vis-NIR, IR, and Raman spectroscopy data were obtained using a Perkin-Elmer Lambda-19 spectrophotometer, a Thermo scientific Nicolet 6700 spectrometer, and a Jasco RMP-210S microscope with an Ar-laser excitation source at 532 nm, respectively. The synthesized 2T-AuNP samples were measured in a DMF solution to obtain the UV-vis-NIR data and KBr pellets for the IR and Raman data, respectively. The UV-vis-NIR data of the assembly films were measured on SiO_2 substrates. The IR spectra consisted of 64 accumulations with a resolution of 4 cm^{-1} using an mercury cadmium telluride detector.

C. Fabrication and transport properties of the 2T-AuNP assemblies

SiO_2 substrates (VIOSIL, KEN-SX) with a flatness of <0.2 nm per 1 μm^2 were obtained from Shin-Etsu Chemical Co. Ltd., Japan. Gold electrodes with a thickness and a gap of 50 nm and 30 μm, respectively, and a width of 9 mm were deposited onto SiO_2 substrates using vacuum evaporation. The SiO_2 substrates coated with the gold electrodes were placed in a glass vial containing 50 ml of a colloidal DMF solution of 2T-AuNP (0.01 mg/ml). The solvent was evaporated at 40 °C in a vacuum to fabricate the 2T-AuNP assembly films. Electrical contacts were formed using carbon paste and were used to attach 25 μm ϕ gold wires. Temperature-dependent dc resistance and current-voltage (*I-V*) characteristics were measured using a homemade cryostat with a temperature control system over the range 300–4.2 K. The current was monitored using a Keithley 6517 electrometer with a constant bias voltage in the range −5 to +5 V. Measurements were carried out on at least five samples to confirm the reproducibility. The relative dielectric constant of 2T was measured using a two-probe ac impedance method at frequencies in the range 100–1 000 000 Hz (HP 4194A) at room temperature. The electrical contacts were prepared using gold paste (No. 8560, Tokuriki Chemical Research Co. Ltd., Japan) to attach 10 μm ϕ gold wires to the 2T pellet. Atomic force microscopy (AFM) images were obtained using a Seiko SPA 400 with an SPI 3800 probe station operating in the dynamic force mode. Commer-

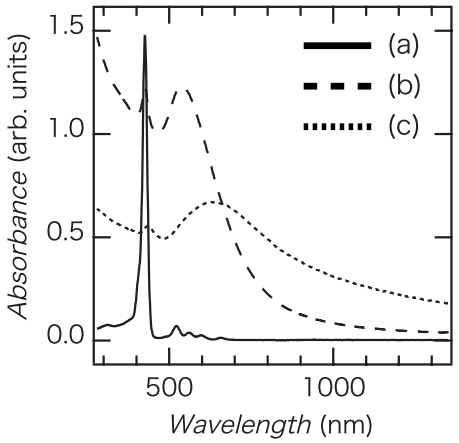

FIG. 1. UV-vis-NIR spectra of (a) 2T, (b) 2T-AuNP nanoparticles measured in a DMF solution, and (c) a 2T-AuNP assembly on an SiO_2 substrate.

cially available Si cantilevers with a force constant of 20 N m^{-1} were used.

III. RESULTS AND DISCUSSION

A. Characterization of 2T-AuNP

A 4 nm diameter spherical gold nanoparticle contains approximately 1750 gold atoms[13] and has a surface area of approximately 50 nm^2. From elemental analysis, a single gold nanoparticle should adsorb approximately 50 molecules of 2T (ratio of 2T:gold atoms=1:33). The cross-sectional area of a 2T molecule that can be adsorbed on a 4 nm gold nanoparticle was estimated to be 1.73 nm^2 and 0.78 nm^2, respectively, for the flat and edge-on configurations [see Fig. S4 (Ref. 11)]. These corresponded to 29 and 64 molecules, respectively. The 50 molecules adsorbed on a 4 nm gold nanoparticle implies that the 2T molecules were adsorbed with a tilted conformation on the gold surface.

B. Adsorption mechanism between 2T and gold nanoparticles

The interaction between gold nanoparticles and 2T on adsorption was examined. The 2T-AuNP exhibited Soret bands in UV-vis-NIR spectrum originating from the 2T [Fig. 1(a)] and plasmon bands of the gold nanoparticles occurring at 426 nm and 539 nm, respectively [Fig. 1(b)]. The Q band, corresponding to the highest occupied molecular orbital-lowest unoccupied molecular orbital transition of 2T, was not observed due to the strong plasmon band. The 2T Soret band did not change after fabrication of a 2T-AuNP indicating that no distortion of the macrocycle ring (redshift),[14] J or H aggregation (redshift or blueshift),[15] charge transfer (redshift),[16] or protonation (redshift) (Ref. 17) of the 2T occurred on the gold surface. The electronic structure of 2T was maintained on formation of the 2T-AuNP. The plasmon band of the gold nanoparticles did not change up to a period of 4 h [Fig. S5 (Ref. 11)], showing the stability of the 2T-AuNP.[18] All the ^{1}H-NMR peaks of 2T-AuNP were significantly broadened [Fig. S6 (Ref. 11)], indicating that the 2T molecules were closely bound to the gold surface.[19]

The adsorption mechanism between the 2T and gold nanoparticles was investigated to ascertain whether it had a covalent or noncovalent nature. Ohta *et al.*[20] reported the possibility of a cleavage of the C-S bond, resulting in an Au-S bond when thiophene is adsorbed on a gold surface. We measured the IR and Raman spectra to confirm the molecular structure of 2T on the gold nanoparticles [see Fig. S7 (Ref. 11)]. The IR spectra showed the C-H stretching mode of thiophene (3098 and 3062 cm^{-1}) (Ref. 21) without the alkyl C-H stretching mode of butane thiol (occurring around 2900 cm^{-1}) expected to be formed by cleavage of the C-S bond of the thiophene ring. Since neither the IR nor the Raman spectra showed any change on adsorption, the adsorption of 2T on the gold nanoparticles was assumed to have a noncovalent bonding nature. Therefore, we propose that the gold nanoparticles can be protected by 2T via physisorption.

C. Fabrication of a 2T-AuNP assembly

Figure 1(c) shows the UV-vis-NIR transmission spectrum of a 2T-AuNP assembly fabricated on an SiO_2 substrate. The Soret and plasmon bands were shifted to the red (from 426 nm and 540 nm to 436 nm and 643 nm, respectively) and were broadened owing to nanoparticle aggregation.[22] The IR spectra [Fig. S7 (Ref. 11)] showed C-H stretching mode of thiophene (3098 and 3062 cm^{-1}) without alkyl C-H stretching mode of TOAB (at around 2900 cm^{-1}), indicating TOAB molecules did not exist in 2T-AuNP, although Schiffrin *et al.*[23] have pointed out the difficulty of removing TOAB from AuNPs. AFM images of a 2T-AuNP assembly between the electrode gap were obtained after charge transport measurements, as shown in Fig. 2. The gold nanoparticles were confirmed to have a rounded shape and an aggregated structure was formed between electrodes. The observed particle diameter (~100 nm) was significantly larger than the estimated value from the TEM and SAXS measurement because the radius of curvature of the cantilevers (approximately 10 nm) was much larger than the particle size (approximately 4 nm). The height of a single 2T-AuNP assembly was confirmed to be about 5 nm [Fig. S8 (Ref. 11)], suggesting that the particle size was maintained in the 2T-AuNP aggregated structure. The height of the network was greater than 50 nm, the electrode height, indicating that the 2T-AuNP assembly had a three-dimensional structure.

D. Temperature dependence of the charge transport of a 2T-AuNP assembly structure

Figure 3 shows temperature-dependent normalized resistance of an assembly structure of 2T-AuNP. The resistivity showed a semiconducting behavior from room temperature to 50 K and was described by an Arrhenius plot (T^{-1}) with the activation energy of 15 meV. This magnitude is of the same order as the assemblies reported previously with similar particle diameters.[24] Ohmic *I-V* characteristics were also confirmed at each measurement point [Fig. S9 (Ref. 11)]. Thermal activated hopping dominated the temperature range between 296 and 50 K. On the other hand, the resistivity below 50 K showed a deviation from the T^{-1} plot. So far,

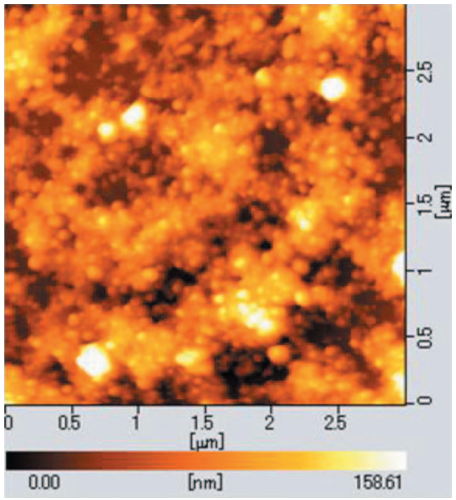

FIG. 2. (Color) AFM images of a 2T-AuNP assembly obtained within the electrode gap after charge transport measurements.

semiconducting charge transport behavior in nanoparticle assemblies has been reported to often obey the VRH model,

$$R \propto \exp\left[\left(\frac{T_0}{T}\right)^{\gamma}\right], \tag{1}$$

where T_0 is a constant and the value of γ depends on the dimensionality. If strong Coulomb interactions exist, then the system obeys a $\gamma=1/2$ law, which is independent of the dimensionality, and is known as ES-VRH.[25,26] The $T^{-1/2}$ plot for a 2T-AuNP assembly is shown in Fig. 3, and indicates a linear relationship existed below 50 K, with a kink in the graph occurring around 10 K.

Below 10 K, the behavior again deviated from the ES-VRH behavior. The *I-V* characteristics were measured at 4.2 K to elucidate the transport mechanism below 10 K. The *I-V* characteristics at 4.2 K showed a threshold behavior (Fig. 4). This behavior can be explained by the model of Middleton and Wingreen (the MW model),[27] which is based on an electron transfer through the nanoparticle assembly taking into account randomly charged nanoparticles separated by tunnel junctions. The *I-V* characteristics of this model are

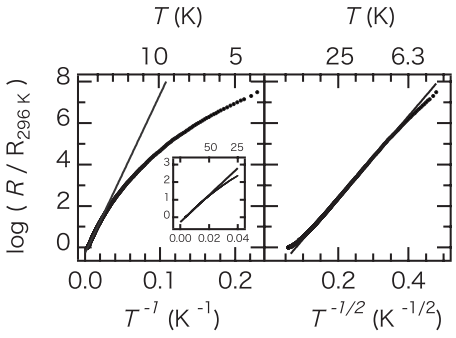

FIG. 3. Normalized resistivity of a 2T-AuNP assembly plotted vs T^{-1} and $T^{-1/2}$. The solid lines denote linear fits in the temperature range 265–50 K (left) and 50–10 K (right).

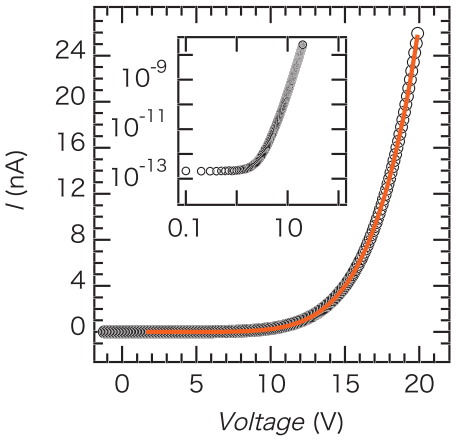

FIG. 4. (Color) *I-V* characteristics of a 2T-AuNP assembly at 4.2 K. The red line denotes the MW model given by Eq. (2). The parameters V_T and ξ were 1.6 V and 6.0 V, respectively. The inset shows the log-log plots.

$$I \propto (V/V_T - 1)^{\xi}, \tag{2}$$

where V_T is the Coulomb-blockade threshold voltage and ξ is the dimensionality of the current pathway, which depends on the structure. The values of $\xi=1$ and 5/3 were calculated for infinite one-dimensional and two-dimensional arrays, respectively, and numerical studies indicated that $2.2<\xi<3.0$ for multilayered arrays.[28] The model reproduced the *I-V* characteristics at 4.2 K well, indicating that electrons can tunnel through the nanoparticles affected by the Coulomb blockade, although the parameter ξ was substantially larger than the theoretical value.

E. Electron transport mechanism

The application of the ES-VRH model to granular systems sometimes results in a hopping distance (r_{hop}) with physically unreasonable values, i.e., hundreds of nanometer or larger,[29] which cannot explain how the Coulomb interactions between the initial and final nanoparticles correlate. To confirm the applicability of the ES-VRH model,[25] we estimated the values of localization length (a) (Refs. 26, 30, and 31) and the r_{hop} (Refs. 29 and 30) of the conduction electrons from

$$T_0 = \beta \frac{e^2}{4\pi\varepsilon_r\varepsilon_0 k_B a}, \tag{3}$$

$$\kappa = \frac{1}{a}, \tag{4}$$

$$r_{hop} = \frac{1}{4\kappa}\left(\frac{T_0}{T}\right)^{1/2}, \tag{5}$$

where κ is the tunneling decay constant, k_B is the Boltzmann constant, e is the electron charge, ε_0 is the dielectric constant in a vacuum, and ε_r is the relative dielectric constant of the surrounding medium. The coefficient β depends on the dimensionality (for two dimensions ~6.5, and for three dimensions ~2.8).[32]

We assumed that a three-dimensional current pathway was realized due to the structural features seen in the AFM images (Fig. 2). From Eqs. (1) and (3), we obtained $a=1.5$ nm ($T=50-10$ K, $T_0=2077$ K, and $\varepsilon_r=15$ obtained from dielectric measurements on 2T). The parameter a describes the decay length of the electronic wave functions. In nanoparticle arrays, the magnitude of a is equivalent to the size of each nanoparticle,[27,33] and larger values imply stronger coupling of the nanoparticles.[31] In the temperature range 50–10 K, the value of r_{hop} increased with decreasing temperature, from 2.4 to 5.4 nm. These distances were relatively small and are physically reasonable when compared with those of earlier reports.[29] Because the 2T-AuNP assemblies contained nanoparticles with a diameter of approximately 4 nm, the increase in the value of r_{hop} from a value of 2.4 nm represents the crossover point of the charge transport mechanism from an Arrhenius-type thermal-activated hopping (i.e., nearest-neighbor hopping) to an ES-VRH-type hopping mechanism around 50 K. The localization length of $a=1.5$ nm indicates that a single electron could be localized within a single nanoparticle and that a single gold nanoparticle in a 2T-AuNP assembly could be in the charged state in the regime of the so-called single-electron charging effect,[34,35] i.e., below 50 K. It is worth noting that, as shown in Fig. 2, the 2T-AuNP were assembled in the form of a continuous multilayer film with many empty spaces between the relatively large electrodes gap (30 μm) compared to the other reports in which closely packed nanoparticle monolayer or multilayer with no empty spaces were created between the gap of 500–600 nm (Ref. 31) and 2–5 μm.[26] The physically reasonable estimated values of localization length a and the r_{hop} suggests appropriateness of ES-VRH-type hopping mechanism in 2T-Au assemblies.

The Coulomb-blockade behavior observed in the I-V characteristics at 4.2 K implies that single-electron tunneling occurred below 10 K. Single-electron tunneling is essentially independent of temperature because it can be realized when the charging energy can overcome the thermal energy.[34] The reason why the $T^{-1/2}$ dependence decreases below 10 K, as shown in Fig. 3, is because of the contribution of the Coulomb blockade. The large value of ξ obtained in the I-V characteristics at 4.2 K strongly suggests a contribution of the ES-VRH-type hopping, although further study will be required.

Some studies have explained the $T^{-1/2}$ behavior using a coherent tunneling model or a random resistance model. The coherent tunneling model was proposed to explain long-range hopping in nanoparticle assemblies.[31] In this model, an electron tunnels into a nanoparticle and another electron escapes from the same nanoparticle at the same time. Coherent tunneling provides a conduction channel at low applied bias through several junctions, where otherwise the Coulomb blockade would suppress any current flow.[36] This behavior is observed in a system with covalent bonds between the gold nanoparticles and an organic molecule, such as a saturated[31] or conjugated molecule.[3] Coherent tunneling is characterized by a power-law I-V behavior in the Coulomb-blockade regime, although only a strong current suppression below V_T (1.6 V) was observed in the present system. In the case of a random resistance model, where $T^{-1/2}$ behavior was the result of a percolation pathway with least resistance, the resistivity behavior only depends on its geometry.[37] If the random resistance model dominates, then the temperature dependence should follow a T^{-1} or $T^{-1/2}$ behavior over the entire temperature range. The resistivity of a 2T-AuNP assembly having a crossover from T^{-1} to $T^{-1/2}$ behavior around 50 K cannot be explained using the random resistance model.

IV. CONCLUSIONS

We have synthesized gold nanoparticles with an average diameter of 4.0 nm protected by physisorbed 2T, which were fabricated into an assembly structure of 2T-AuNP. We fabricated assemblies of gold nanoparticles protected by a π-conjugated molecules via noncovalent bonding and measured their electronic transport properties. On lowering the temperature, the temperature-dependent resistivity of a 2T-AuNP assembly structure showed a crossover from an Arrhenius-type thermal-activated hopping to an ES-VRH-type hopping mechanism around 50 K. In addition, a Coulomb blockade influenced the strong Coulomb repulsion between the nanoparticles below 10 K. The existence of a crossover is supported by the hopping distance of 2.4 nm at 50 K, which implies that the hopping distance between nearest-neighbor particles increases to 5.4 nm at 10 K. The localization length of 1.5 nm estimated from the ES-VRH model was smaller than the 2T-AuNP diameter, indicating a weak coupling between NP units and the single-electron charging effect. Below 10 K, the Coulomb-blockade behavior caused a smaller temperature dependence of the resistivity. The appearance of the ES-VRH behavior and the Coulomb-blockade behavior indicated that the 2T and gold nanoparticles in the 2T-AuNP assembly were electrically isolated from each other, although the gold nanoparticles were surrounded by an electrically active organic molecule. This was due to the weak adsorption of 2T on the gold nanoparticles via physisorption.

ACKNOWLEDGMENTS

This work was supported in part by a Grant-in-Aid for Science Research from the Ministry of Education, Culture, Sports, Science, and Technology of Japan. Y.N. acknowledges Japan Society for the Promotion of Science (JSPS).

[1] A. Zabet-Khosousi, P. E. Trudeau, Y. Suganuma, A. A. Dhirani, and B. Statt, Phys. Rev. Lett. **96**, 156403 (2006); J. B. Pełka, M. Brust, P. Gierłowski, W. Paszkowicz, and N. Schell, Appl. Phys. Lett. **89**, 063110 (2006).

[2] H. Nakanishi, K. J. M. Bishop, B. Kowalczyk, A. Nitzan, E. A. Weiss, K. V. Tretiakov, M. M. Apodaca, R. Klajn, J. F. Stoddart, and B. A. Grzybowski, Nature (London) **460**, 371 (2009); X. N. Xie, Y. Xie, X. Gao, C. H. Sow, and A. T. S. Wee, Adv. Mater. **21**, 3016 (2009).

[3] M. Minamoto, M. M. Matsushita, and T. Sugawara, Polyhedron **24**, 2263 (2005); P. Nickels, M. M. Matsushita, M. Minamoto, S. Komiyama, and T. Sugawara, Small **4**, 471 (2008); T. Sugawara, M. Minamoto, M. M. Matsushita, P. Nickels, and S. Komiyama, Phys. Rev. B **77**, 235316 (2008).

[4] M. Brust, M. Walker, D. Bethell, D. J. Schiffrin, and R. Whyman, J. Chem. Soc., Chem. Commun. 1994, 801; M. Brust, J. Fink, D. Bethell, D. J. Schiffrin, and C. Kiely, *ibid.* **1995**, 1655.

[5] V. Torma, O. Vidoni, U. Simon, and G. Schmid, Eur. J. Inorg. Chem. **2003**, 1121 (2003).

[6] J. M. Wessels, H.-G. Nothofer, W. E. Ford, F. von Wrochem, F. Scholz, T. Vossmeyer, A. Schroedter, H. Weller, and A. Yasuda, J. Am. Chem. Soc. **126**, 3349 (2004).

[7] F. Chen, X. Li, J. Hihath, Z. Huang, and N. Tao, J. Am. Chem. Soc. **128**, 15874 (2006).

[8] N. J. Tao, Nat. Nanotechnol. **1**, 173 (2006).

[9] A. D. Adler, F. R. Longo, J. D. Finarelli, J. Goldmacher, J. Assour, and L. Korsakoff, J. Org. Chem. **32**, 476 (1967).

[10] MERCURY Version 2.3, The Cambridge Crystallographic Data Centre, UK., IMAGEJ Version 1.43u, The National Institutes of Health, USA.

[11] See supplementary material at http://link.aps.org/supplemental/10.1103/PhysRevB.82.205420 for supporting figures.

[12] M. J. Frisch *et al.*, Gaussian, Inc., Wallingford, CT, 2004.

[13] G. Schmid, Chem. Rev. **92**, 1709 (1992).

[14] J. P. Hill, I. J. Hewitt, C. E. Anson, A. K. Powell, A. L. McCarty, P. A. Karr, M. E. Zandler, and F. D'Souza, J. Org. Chem. **69**, 5861 (2004).

[15] M. Zhou, S. Ouyang, Z. Liu, G. Lu, S. Gao, and Z. Li, Vib. Spectrosc. **49**, 7 (2009); M. Gouterman, D. Holten, and E. Lieberman, Chem. Phys. **25**, 139 (1977); J. Zimmermann, U. Siggel, J.-H. Fuhrhop, and B. Roder, J. Phys. Chem. B **107**, 6019 (2003); K. A. Scherz and W. W. Parson, Biochim. Biophys. Acta **766**, 653 (1984).

[16] A. Hosseini, S. Taylor, G. Accorsi, N. Armaroli, C. A. Reed, and P. D. W. Boyd, J. Am. Chem. Soc. **128**, 15903 (2006).

[17] I. Gupta and M. Ravikanth, J. Photochem. Photobiol., A **177**, 156 (2006).

[18] S. K. Ghosh and T. Pal, Chem. Rev. **107**, 4797 (2007); M. M. Maye, J. Luo, I-I. S. Lim, L. Han, N. N. Kariuki, D. Rabinovich, T. Liu, and C.-J. Zhong, J. Am. Chem. Soc. **125**, 9906 (2003); J. A. Creighton, C. G. Blatchford, and M. G. Albrecht, J. Chem. Soc., Faraday Trans. 2 **75**, 790 (1979); K. U. von Raben, R. K. Chang, and B. L. Laube, Chem. Phys. Lett. **79**, 465 (1981); S. Link and M. A. El-Sayed, J. Phys. Chem. B **103**, 8410 (1999).

[19] C. Mayer, Annu. Rep. NMR Spectrosc. **55**, 205 (2005).

[20] E. O. Sako, H. Kondoh, I. Nakai, A. Nambu, T. Nakamura, and T. Ohta, Chem. Phys. Lett. **413**, 267 (2005).

[21] T. Matsuura and Y. Shimoyama, Eur. Phys. J. E **7**, 233 (2002).

[22] A. M. Kalsin, A. O. Pinchuk, S. K. Smoukov, M. Paszewski, G. C. Schatz, and B. A. Grzybowski, Nano Lett. **6**, 1896 (2006); A. O. Pinchuk, A. M. Kalsin, B. Kowalczyk, G. C. Schatz, and B. A. Grzybowski, J. Phys. Chem. C **111**, 11816 (2007).

[23] C. A. Waters, A. J. Mills, K. A. Johnson, and D. J. Schiffrin, Chem. Commun. (Cambridge) 2003, 540.

[24] For example, 38 meV for 4.6–6.5 nm diameter, R. Parthasarathy, X. M. Lin, K. Elteto, T. F. Rosenbaum, and H. M. Jaeger, Phys. Rev. Lett. **92**, 076801 (2004); 20 meV for 6 nm diameter, M. Brust, D. Bethell, C. J. Kiely, and D. J. Schiffrin, Langmuir **14**, 5425 (1998); 47–58 meV for 4 nm diameter, Y. Joseph, I. Besnard, M. Rosenberger, B. Guse, H. G. Nothofer, J. M. Wessels, U. Wild, A. Knop-Gericke, D. Su, R. Schlögl, A. Yasuda, and T. Vossmeyer, J. Phys. Chem. B **107**, 7406 (2003).

[25] A. L. Efros and B. I. Shklovskii, J. Phys. C **8**, L49 (1975); B. I. Shklovskii and A. L. Efros, *Electronic Properties of Doped Semiconductors* (Springer-Verlag, Berlin, 1988).

[26] D. Yu, C. Wang, B. L. Wehrenberg, and P. Guyot-Sionnest, Phys. Rev. Lett. **92**, 216802 (2004); B. L. Wehrenberg, D. Yu, J. Ma, and P. Guyot-Sionnest, J. Phys. Chem. B **109**, 20192 (2005); H. E. Romero and M. Drndic, Phys. Rev. Lett. **95**, 156801 (2005).

[27] A. A. Middleton and S. N. Wingreen, Phys. Rev. Lett. **71**, 3198 (1993).

[28] C. T. Black, C. B. Murray, R. L. Sandstrom, and S. Sun, Science **290**, 1131 (2000); H. Fan, K. Yang, D. M. Boye, T. Sigmon, K. J. Malloy, H. Xu, G. P. López, and C. Jeffrey Brinker, *ibid.* **304**, 567 (2004).

[29] J. L. Dunford, Y. Suganuma, A.-A. Dhirani, and B. Statt, Phys. Rev. B **72**, 075441 (2005); T. Dadosh, Y. Gordin, R. Krahne, I. Khivrich, D. Mahalu, V. Frydman, J. Sperling, A. Yacoby, and I. Bar-Joseph, Nature (London) **436**, 677 (2005); Z.-M. Liao, J. Xun, and D.-P. Yu, Phys. Lett. A **345**, 386 (2005); M. A. Rafiq, Y. Tsuchiya, H. Mizuta, S. Oda, S. Uno, Z. A. K. Durrani, and W. I. Milne, J. Appl. Phys. **100**, 014303 (2006).

[30] A. Zabet-Khosousi and A. A. Dhirani, Chem. Rev. **108**, 4072 (2008).

[31] T. B. Tran, I. S. Beloborodov, X. M. Lin, T. P. Bigioni, V. M. Vinokur, and H. M. Jaeger, Phys. Rev. Lett. **95**, 076806 (2005); D. V. Averin and Y. V. Nazarov, *ibid.* **65**, 2446 (1990).

[32] K. Xu, L. Qin, and J. R. Heath, Nat. Nanotechnol. **4**, 368 (2009); V. Duc Nguyen, V. Lien Nguyen, and D. Toi Dang, Phys. Lett. A **349**, 404 (2006).

[33] K. C. Beverly, J. F. Sampaio, and J. R. Heath, J. Phys. Chem. B **106**, 2131 (2002).

[34] M. Amman, R. Wilkins, E. Ben-Jacob, P. D. Maker, and R. C. Jaklevic, Phys. Rev. B **43**, 1146 (1991).

[35] B. Abeles, P. Sheng, M. D. Coutts, and Y. Arie, Adv. Phys. **24**, 407 (1975).

[36] I. S. Beloborodov, A. V. Lopatin, and V. M. Vinokur, Phys. Rev. B **72**, 125121 (2005).

[37] V. Ambegaokar, B. I. Halperin, and J. S. Langer, Phys. Rev. B **4**, 2612 (1971); K.-H. Müller, J. Herrmann, B. Raguse, G. Baxter, and T. Reda, *ibid.* **66**, 075417 (2002); K.-H. Müller, G. Wei, B. Raguse, and J. Myers, *ibid.* **68**, 155407 (2003).